Model-based Approach to Tissue Characterization using Optical Coherence Tomography

Cecília Lantos[1,2,3], Rafik Borji[1], Stéphane Douady[2], Karolos Grigoriadis[1], Kirill Larin[4] and Matthew A. Franchek[1]

[1]*Department of Mechanical Engineering, University of Houston, 4800 Calhoun Road, Houston, TX 77004, U.S.A.*
[2]*Laboratory of Matter and Complex Systems, Paris Diderot University, 5 Rue Thomas Mann, Paris, 75013, France*
[3]*Department of Hydrodynamic Systems, Budapest University of Technology and Economics, Műegyetem Rakpart 3-9, Budapest, 1111, Hungary*
[4]*Department of Biomedical Engineering, University of Houston, 4800 Calhoun Road, Houston, TX 77004, U.S.A.*

Keywords: Optical Coherence Tomography, Tissue Characterization, Medical Diagnostics, Cancer, Liposarcoma, Model-based, Imaging.

Abstract: Structural property of the tissue can be quantified by its optical scattering properties. Since a tumor is differentiated from healthy tissue based on morphological analysis, model-based approach to cancer diagnosis is developed. The scattering property is measured using Optical Coherence Tomography. The structural subsurface images from the measurements are described quantitatively. A parametric model is developed to classify tissue as healthy or cancerous. A statistical model-based imaging method is created to distinguish healthy vs. cancerous soft tissue using the example of human Normal Fat vs. Well-Differentiated- (WD-), and De-Differentiated Liposarcoma (DDLS).

1 INTRODUCTION

Characteristics of tissue structural properties are studied non-invasively with different imaging modalities (Magnetic Resonance Imaging, Computed Tomography, Ultrasound, Optical Coherence Tomography …) (Rembielak, 2011; Morris, 2012). Each works at different scale depending on interest based on different physical principles using specific frequency range of the electromagnetic spectrum (radio frequency-, X-ray, sound-, light wave…). These techniques can be coupled for multidisciplinary analysis of the tissue providing different information detected from backscattered waves from the internal structure. The outputs of these backscattered signals are grayscale images with different resolution and imaging depth revealing the subsurface structure (Rembielak, 2011; Morris, 2012).

We chose Optical Coherence Tomography (OCT) to analyze tissue structural properties. OCT records images based on near infrared (NIR) laser light scattered back from the tissue (Drexler, 2008, Brezinski, 2006). Instead of subjective image analysis, we approach the diagnosis from mathematical point of view in order to quantify topological changes. We develop a simple statistical model based on the images analyzing the scattering properties distinguishing various tissue types. The tissue example is Normal Fat tissue vs. Well-differentiated and De-differentiated Liposarcoma, but the idea can be broadened toward the analysis of other type of cancer since the diagnosis is based on morphology. This model based imaging can become a clinical tool to provide a second opinion for physiologists.

In the literature, some approaches have been elaborated that could differentiate quantitatively between the various tissue types and specifically between healthy and cancerous tissue recorded with OCT. The attenuation of backscattered laser light in function of depth (z) in the biological material theoretically follows an exponential function (Drexler, 2008; Brezinski, 2006):

$$I(z) = I_0 e^{-u_t z} \quad (1)$$

defined by the scattering coefficient u_t characterizing different tissue types, calculating from the slope of the intensity attenuation in dB scale. This implies the abstraction of the tissue

Lantos C., Borji R., Douady S., Grigoriadis K., Larin K. and A. Franchek M..
Model-based Approach to Tissue Characterization using Optical Coherence Tomography.
DOI: 10.5220/0004805500190027
In *Proceedings of the International Conference on Bioimaging* (BIOIMAGING-2014), pages 19-27
ISBN: 978-989-758-014-7

structure. For inhomogeneous material the slope is calculated by averaging or filtering, and the analysis of the deviation from the slope characterizes well the tissue (Lev, 2011, Yang, 2011, McLaughlin, 2010, Mujat, 2009, Goldberg, 2008).

Morphological pattern of breast cancer in OCT images has been studied by fractal analysis using box-counting algorithm (Sullivan, 2011). The periodicity analysis based on the scattering effect due at the cell boundaries distinguishes healthy vs. cancerous breast tissue (Zysk, 2006; Mujat, 2009; Goldberg, 2008). A similar method based on cell counting is already applied on OCT images of Liposarcoma (Carbajal, 2011).

Speckle phenomena are a random scattering effect, called texture, which analysis reveals the tissue types in case of inadequate structural resolution (Gossage, 2003; Gossage, 2006).

2 TISSUE STRUCTURE RECORDED WITH OPTICAL COHERENCE TOMOGRAPHY

Optical Coherence Tomography (OCT) is a well-known structural imaging method applied on biological material, in particular for cancer diagnosis (Drexler, 2008, Brezinski, 2006). OCT has a better resolution (3-10 μm) compared to other diagnostic methods, revealing the subsurface structure in a 1-3 mm deep region under the surface, and has proved to be the most suitable imaging method applied on Liposarcoma (Carbajal, 2011; Lahat, 2009; Lev, 2011).

According to the WHO report on Soft tissue tumors, Liposarcoma is part of the Adipocytic Tumors. In this study we differentiate Normal Fat from Intermediate (locally agressive) tumor, so called Well-Differentiated Liposarcoma (WDLS) and from one type of Malignant tumor (having risk to metastasize), called De-Differentiated Liposarcoma (DDLS) (Fletcher, 2006).

Tissue samples were excised from human patients' abdomen/retroperitoneum at the University of Texas M. D. Anderson Cancer Center (UTMDACC). Protocols for tissue processing were approved by the UTMDACC and University of Houston Biosafety Committees. Histological diagnosis and classification of samples was performed by a UTMDACC sarcoma pathologist. The tissue was put in sterile phosphate buffered saline then stored in refrigerator until imaged with the OCT system.

We record the tissue on a Spectral-Domain (SD) OCT measuring rig in the BioOptics Laboratory at the University of Houston. A supraluminescent laser diode (Superlum, S840-B-I-20) generates a broadband laser signal with center wavelength at λ_0 = 840 nm, spectral bandwidth at $\Delta\lambda$ = 50 nm and output power at 20 mW (Carbajal, 2011) (Figure1).

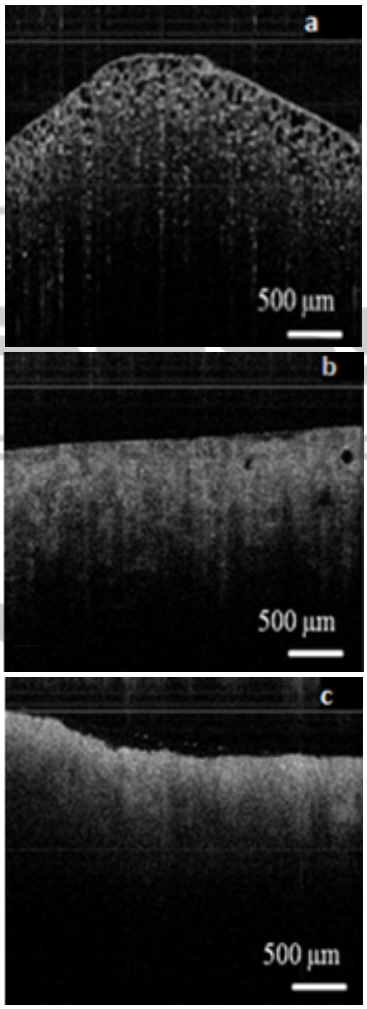

Figure 1: a) Normal Fat Tissue cross-section OCT image (mature fat, adipose cells), logarithmic response. b) Well-differentiated Fat Tissue cross-section OCT image (WDLS with extensive myxoid change), logarithmic response. c) De-differentiated Fat Tissue cross-section OCT image (Highly fibrotic DDLS), logarithmic response.

The above images show the cross-section of Human Normal Fat tissue (Figure 1a), WDLS (Figure 1b) and DDLS (Figure 1c). This 2D cross-section called B-scan is composed of 500 adjacent A-lines. One A-line (1D) shows the backscattered intensity variation in function of depth from a laser footprint of 8 μm in focal plane. The region is 3mm

wide scanned with a galvanometer mirror, with backscattered light collected from a region of up to ~1 mm in depth.

The internal structure is revealed. We can see the differences of the different tissue types on the gray-scale images. We intend to transform the qualitative information from the images to a quantitative statistical parametric description of the tissue. The statistical model is based on the variability of the A-lines in the cross-section at a given region. One A-line of the different tissue types is seen on Figure 2.

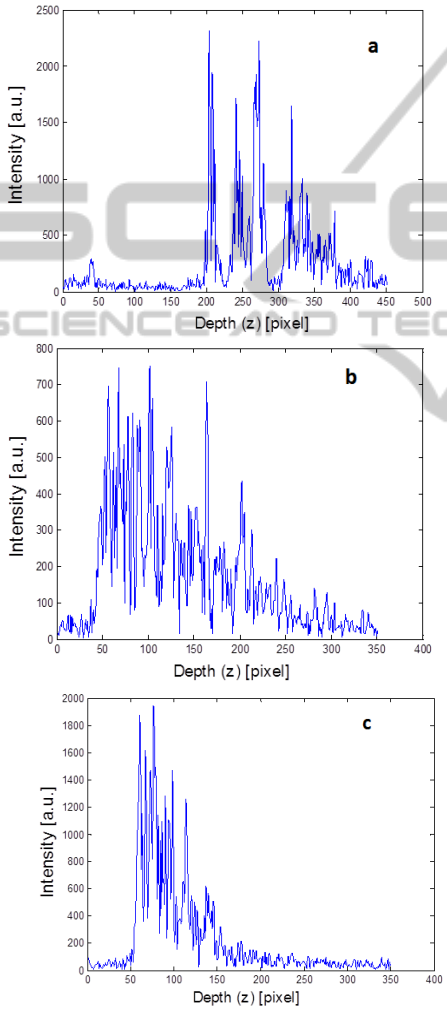

Figure 2: OCT A-line of a) Normal Fat b) WDLS c) DDLS. The intensity of the input laser light and the path-length difference between the reference mirror and the tissue surface differ in each case.

1D imaging (Intensity as a function of depth at a single point) is obtained by applying Digital Signal Processing methods on the data detected on a line scan camera (Basler Sprint L104K-2k, 2048 pixel resolution, 29.2 kHz line rate), -with a resolution of 2k, and a 10x10 μm2 pixel size, detecting 2048 wavelength intensity values between 800-890 nm. The signal is digitized using an analog-to-digital converter (NI-IMAQ PCI-1428). The intensity detected on the line-scan camera is the cross-correlation of the broadband laser light electric field split in a Michelson interferometer and scattered back from a reference mirror and from the sample layers at each frequency component (Carbajal, 2011, Drexler, 2008, Brezinski, 2006). The broadband laser light is decomposed into its spectral components in passing through a diffraction grating (Wasatch Photonics, 1200 grooves/mm). The measurement setting and DSP is computed in Labview, whence the intensity functions as function of depth are analyzed in Matlab.

3 DATA ANALYSIS

The post-processing steps to determine the model on the Fourier-domain signatures derived from OCT data will be explained here. Human Normal Fat, WDLS and DDLS tissue samples will be analyzed. We will focus on the statistical properties of the backscattered intensity signals.

For the computation, the tissue surface should first be numerically straightened. We apply the canny edge detector implemented in Matlab Image Processing Toolbox on the B-scans after median filtering the images. This can be used to align the scans, but does not yield the absolute position of the surface with respect to common origin. Before further analysis we screen all the B-scans to verify that each one is straightened properly.

At each depth position the mean and standard deviation of the intensity signals will be calculated. Then, attenuation effects are removed from the data by dividing the Intensity Values or the standard deviation of the A-lines by the mean from each backscattered intensity response, so as to normalize every scan line.

The images are corrected according to the normalized camera sensitivity curve, to eliminate the errors coming from the intensity variations because of the oblique tissue surface. It is due to the camera feature recording the same sample point at lower intensity from farther path-length differences following a Gaussian decay (Bajraszewski, 2008).

3.1 Standard Deviation over Mean

In the first case the tissue characterization will be defined from the Probability Density Functions

(PDF) of the STD/MEAN curves. The three-parameter Generalized Extreme Value (GEV) Distribution fits the histograms well due to its high flexibility:

$$y = f(x|k,\mu,\sigma) = \left(\frac{1}{\sigma}\right)\exp\left(-\left(1+k\frac{(x-\mu)}{\sigma}\right)^{-\frac{1}{k}}\right)\left(1+k\frac{(x-\mu)}{\sigma}\right)^{-1} \quad (2)$$

where x is the std/mean of the intemsity values, y is the distribution, k is the shape-, σ is the scale-, μ is the location parameter.

To find the tissue surface on the straightened images the mean of the A-lines in one B-scan, and the first derivatives of the mean are calculated from the uncorrected images. The tissue surface is defined at the highest derivative point.

After the tissue surface is defined, 150 pixel = 0.659 mm is considered for analysis because the most dense tissue (DDLS) does not reflect light from deeper region at this wavelength range and camera settings (Figures 3a).

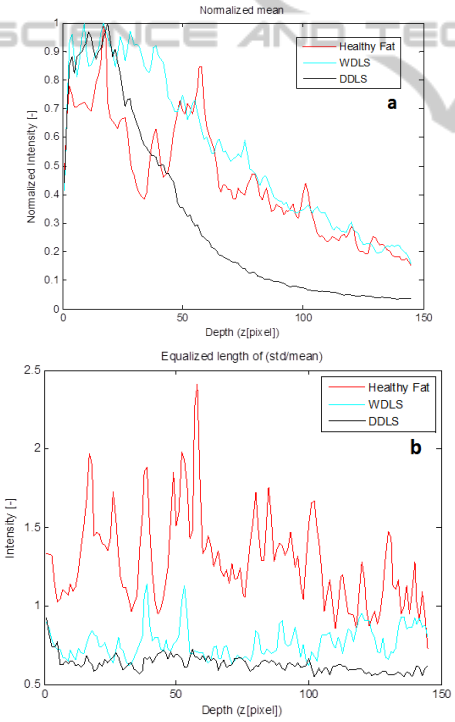

Figure 3: a) Averaged B-scan, mean intensity value at each depth position on Normal Fat, WDLS, DDLS; (150 pixels from the tissue surface) The curves here are normalized according to maximum value only for representation. b) Standard Deviation over Mean at each depth position in the same region.

The next step will be to define the Region of Interest (ROI) on the curves for analysis. This analysis relies on the use of a windowing scheme, in which sections of the intensities as function of depth are evaluated separately.

After evaluation of the data in each window region at each B-scan via the parameters of the GEV distribution, a window size of 40 pixel = 0.1758 mm is chosen, beginning from the tissue surface. Our method turned out to be independent on the surface scattering effect.

To depict the accuracy of the results, 160 WDLS or DDLS and 200 Normal Fat B-scans were analyzed. Figure 4 shows the mean and STD of the GEV parameters on the Gaussian corrected curves. It characterizes well the different tissue types.

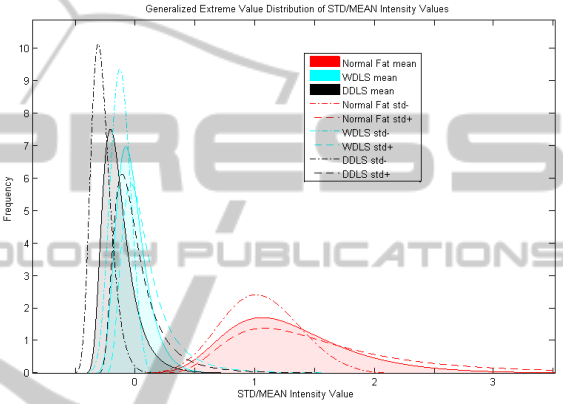

Figure 4: Histogram, GEV Distribution (k, σ, μ) calculated from the STD/mean ratio of the intensity values at each depth position in ROI, mean and standard deviation on 200 B-scans of Normal Fat, and 160 B-scans of WDLS and DDLS.

The curve coefficients well differentiate between the healthy and cancerous tissues, but there is less distinction between the grades of the cancer (Table 1).

Table 1: GEV parameters calculated from the STD/MEAN ratio of the intensity values at each depth position, mean and standard deviation on 200 B-scans of Normal Fat, and 160 B-scans of WDLS and DDLS.

STD/MEAN	k	σ	μ
Baseline (Normal Fat)	0.0007 +0.2347	0.2151 +0.0579	1.2796 +0.0659
Deviation1 (WDLS)	-0.0128 +0.2443	0.0529 +0.0120	0.7093 +0.0359
Deviation2 (DDLS)	0.0857 +0.1673	0.0493 +0.0128	0.6502 +0.0584

To draw the deviation from the baseline tissue the next parameters are calculated, where b is the Baseline tissue parameter, d is the Deviated tissue parameter.

Table 2: Comparison of the GEV parameters calculated from the STD/mean ratio of the intensity values at each depth position, mean and standard deviation on 200 B-scans of Baseline Tissue and 160 B-scans of Deviation 1&2.

STD/MEAN	$\Delta k = \frac{k_d - k_b}{k_b}$	$\Delta \sigma = \frac{\sigma_d - \sigma_b}{\sigma_b}$	$\Delta \mu = \frac{\mu_d - \mu_b}{\mu_b}$
Baseline (Normal Fat)	0 ±335.2857	0 ±0.2692	0 ±0.0515
Deviation 1 (WDLS)	-19.2857 [-368.2857; 329.7143]	-0.7541 [-0.8099; -0.6983]	-0.4457 [-0.4737; -0.4176]
Deviation 2 (DDLS)	121.4286 [-117.5714; 360.4286]	-0.7708 [-0.8303; -0.7113]	-0.4919 [-0.5375; -0.4462]

The next figure represents the coefficient differences on the axes of a 3D coordinate system. It is clear, that there is a relevant separation between the healthy and cancerous tissue in each projection plane.

3.2 Normalized Intensity Variation

A second method is developed to analyze the same data set. Instead of calculating the STD/MEAN, all the measured intensity values are now considered, and also normalized by the mean intensity at each depth position. The same windowing process was applied on the A-lines and B-scans, and the optimal window size of 40 pixels beginning from the surface has been proved. Figure 6 and Table 3 shows the mean and STD of the GEV parameters characterizing the different tissue types.

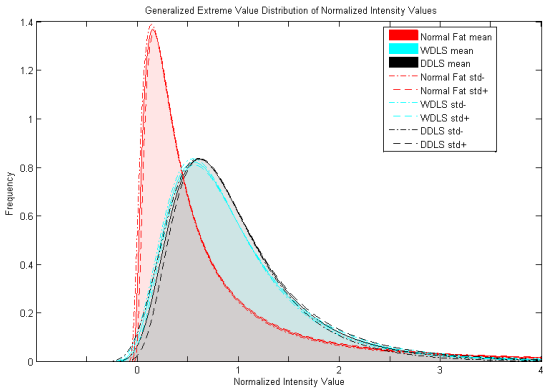

Figure 6: Histogram, GEV Distribution (k, σ, μ) calculated from the mean-normalized intensity values in ROI, mean and standard deviation on 200 B-scans of Normal Fat, and 160 B-scans of WDLS and DDLS.

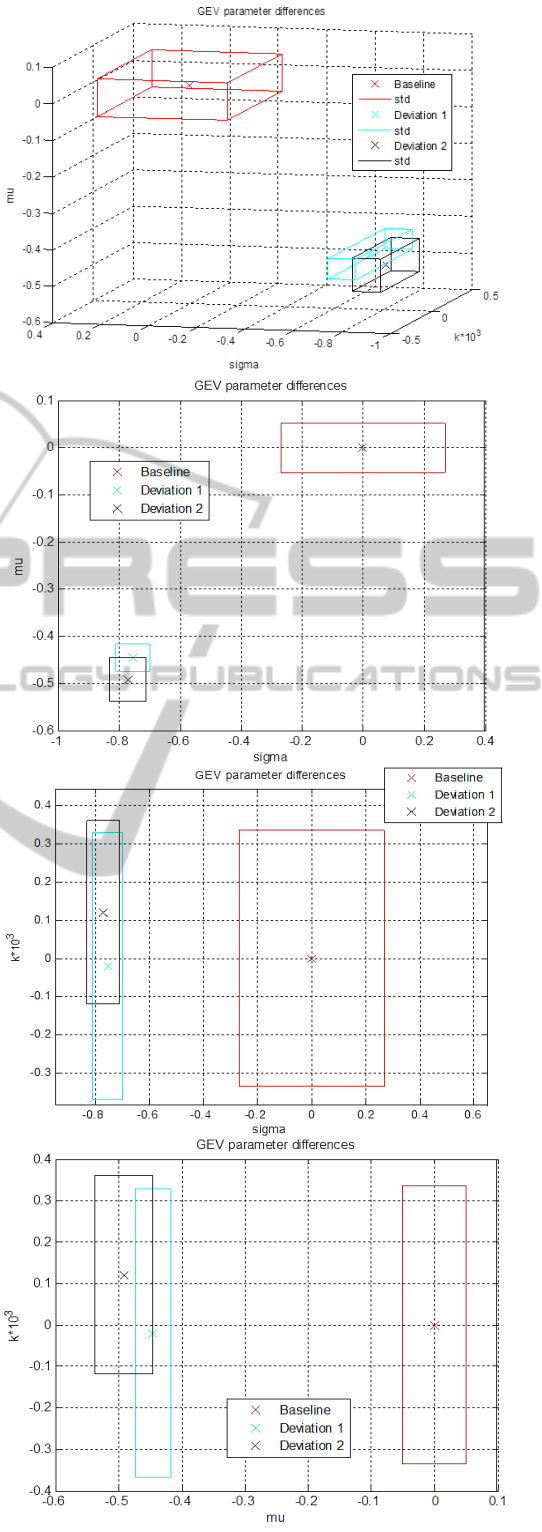

Figure 5: Comparison of the GEV parameters represented at each axe of the 3D coordinate system calculated from the STD/mean ratio of the intensity values at each depth position, mean and standard deviation on 200 B-scans of Baseline Tissue and 160 B-scans of Deviation 1&2.

Similarly to the first method the curve coefficients characterize well the healthy and cancerous tissue but WDLS and DDLS coefficients are not sufficiently distinguished.

Table 3: GEV parameters calculated from the mean-normalized intensity values in ROI, mean and standard deviation on 200 B-scans of Normal Fat, and 160 B-scans of WDLS and DDLS.

I/MEAN	k	σ	μ
Baseline (Normal Fat)	0.8209 +0.0647	0.3532 +0.0181	0.3191 +0.0254
Deviation1 (WDLS)	0.1905 +0.0358	0.4561 +0.0100	0.6381 +0.0229
Deviation2 (DDLS)	0.1447 +0.0684	0.4462 +0.0044	0.6700 +0.0364

The next table shows the deviation from the baseline tissue, where b is the Baseline tissue parameter, d is the Deviated tissue parameter.

Table 4: Comparison of the GEV parameters calculated from the mean-normalized intensity values in ROI, mean and standard deviation on 200 B-scans of Baseline Tissue and 160 B-scans of Deviation 1&2.

ΣI /MEAN	$\frac{\Delta k}{k_b} = \frac{k_d - k_b}{k_b}$	$\frac{\Delta \sigma}{\sigma_b} = \frac{\sigma_d - \sigma_b}{\sigma_b}$	$\frac{\Delta \mu}{\mu_b} = \frac{\mu_d - \mu_b}{\mu_b}$
Baseline (Normal Fat)	0 ±0.0788	0 ±0.0512	0 ±0.0796
Deviation1 (WDLS)	-0.7679 [-0.8115; -0.7243]	0.2913 [0.2630; 0.3196]	0.9997 [0.9279; 1.0715]
Deviation2 (DDLS)	-0.8237 [-0.9071; -0.7404]	0.2633 [0.2508; 0.2758]	1.0997 [0.9856; 1.2137]

The next figure shows similar results then the first method representing the coefficient differences in the 3D coordinate system and separating well the healthy and cancerous tissue in each projection plane, however the different cancer tissues are overlapped.

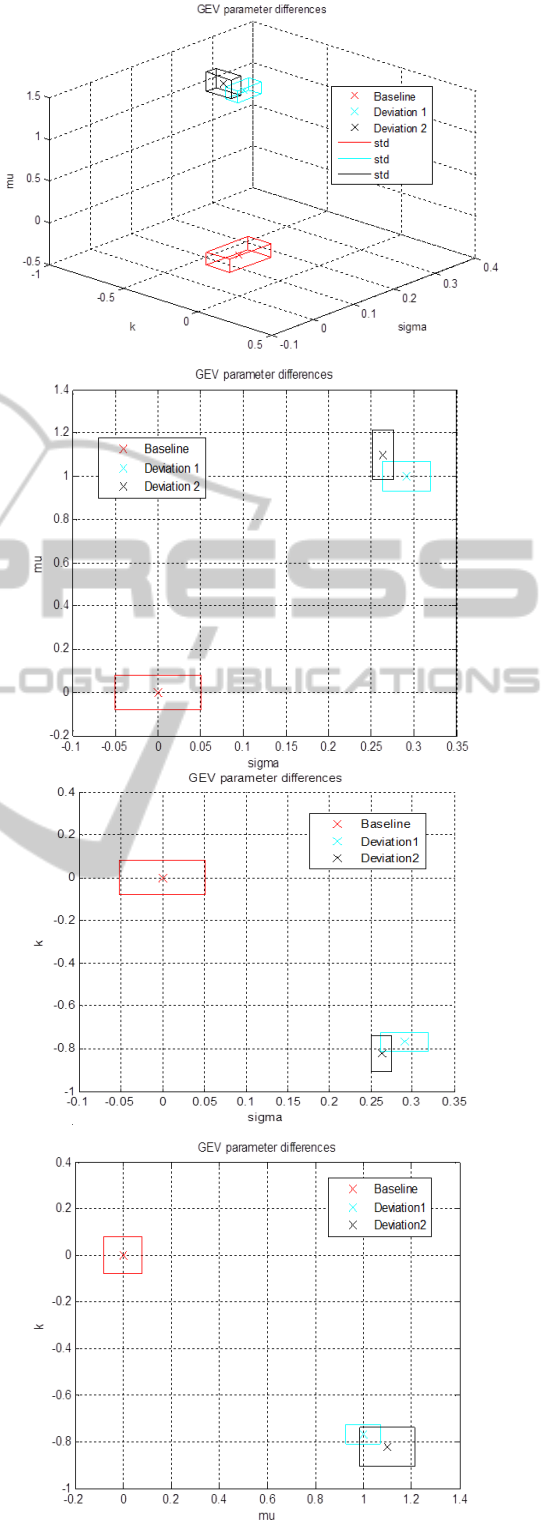

Figure 7: Comparison of the GEV parameters represented at each axe of the 3D coordinate system calculated from the mean-normalized intensity values in ROI, mean and standard deviation on 200 B-scans of Baseline Tissue and 160 B-scans of Deviation 1&2.

4 DISCUSSION

We can deduce that both statistical analyses are a viable method to differentiate tissue types with a good accuracy. The method is independent on the measurement settings as the results are normalized by the mean of the intensity values at each depth position, and errors due to path-length differences are corrected. For comparison the data analysis was also applied on the images without this correction

revealing that only the shape parameter (k) is affected in a non-negligible way in the case the STD/MEAN ratio is calculated. This analysis is more sensitive also to the way how we find the surface of the tissue since the data points from which the histogram is drawn is deduced calculating the STD/MEAN from each depth position (40 pixels), comparing to the second method where the histogram is drawn from the data points contained in all the Region of Interest (40x200 or 40x160 pixel points). In case we want to get absolute parameters, which describe tissue type, the correction is needed.

The method could be developed to distinguish better the different grade of cancer implementing with additional factors, e.g. the mean intensity values at each depth position. The weak point of the measurements is that setting the position of the tissue under the laser light to get a visible subsurface structure is controlled manually. The measurements revealed that the focus position does not affect significantly the quantitative results, but some saturated intensity points can also affect the statistics.

It has already been proved that this non-invasive measurement technique shows good similarities with stained histology (Figure 8) (Lev, 2011). The novelty of our study was to develop a mathematical model-based approach instead of visual grading of the structure to be able to differentiate tissue types.

The structure is detected from the scattering properties of the tissue types. The laser clearly reveals the adipose cells seen in Normal Fat. WDLS has extensive myxoid change including vasculature, but still has some adipose cells with varying size, which is a diagnostic of WDLS. The part of DDLS imaged here resembles fibrotic tissue.

Cancerous tissue is much denser than healthy tissue. Since light scattering occurs chiefly at interfaces, scattering is much stronger in cancerous tissue. The inhomogeneous Normal Fat is distinguished with periodic scattering at the cell boundaries. The attenuation of light is higher in the dense tissue, detectable with the attenuation coefficient u_t, and the back reflection loses the periodicity as the adipose cells dedifferentiate in the cancerous tissue. The optical properties show the morphology of the tissues, the scattering effects reveal the cellular structure at a good resolution for our analysis.

For medium grade sarcoma (WDLS), there is much larger cell size dispersion than in healthy tissue. An analysis of the structure's periodicities is sensitive to this, as well as speckle analysis. Cell counting analysis can reveal the difference between

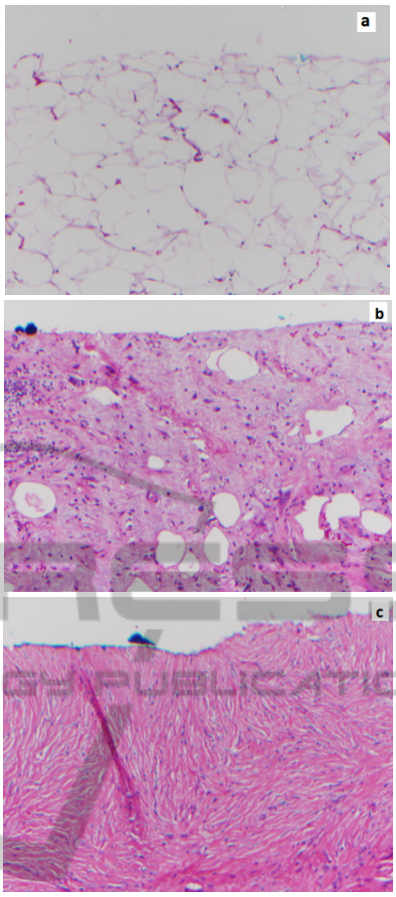

Figure 8: Histological images (Magnification 10x) of a) Normal Fat b) Well-Differentiated Liposarcoma with extensive mitotic change c) Highly Fibrotic De-Differentiated Liposarcoma.

healthy tissue and high grade of cancer (DDLS), the size of the variable adipose cells should be included in the algorithm to distinguish between normal fat and medium grade of cancer (WDLS). It can be improved using artificial network analysis already calculated on histological data (Sjöström, 1999). There is a certain degree of order (on a given length scale) in healthy tissue. On the contrary, in sarcoma, many scales are present, which is revealed by fractal analysis.

The techniques proposed in literature have not been applied in clinical practice yet and there are some shortcomings in the analysis. The slope analysis discards all structural information; the fractal analysis is too complicated and subject to erroneous or ambiguous interpretation due to experimental errors. The speckle analysis discards information on loss of intensity due to multiple scattering events. Finally it seems likely that completely automated, practicable cell counting

analysis will not be achieved using traditional image analysis software.

The aim of our study is to develop a simple analysis technique based on a parametric method that captures the structural features from the strength of scattering. Here only one histological subtype of WDLS and DDLS is described, however they can represent several patterns (Miettinen, 2003, Miettinen, 2010) The comparison of the different histological subtypes and the ability to differentiate from Normal Fat and Lipoma, benign adipose tissue is a future study.

5 CONCLUSIONS

Our objective was to study the response of tissue to a near infrared laser excitation, and, specifically, to characterize differences between healthy and cancerous tissue. The morphology of the subsurface is depicted based on the backscattered near infrared light. Parametric models of these backscattered signal characteristics are derived and linked statistically to the optical properties of Normal Fat, Well-Differentiated Liposarcoma and De-Differentiated Liposarcoma.

The accurate diagnosis at early stage of cancer, as well as the recognition of the tumor boundary in tissue is highly important. However OCT has been well-recognized as a powerful method for cancer detection from tissue morphology, the diagnosis from these images is subjective and not obvious. We intend to fill the need for an objective means of data analysis. The goal of the current study was to develop a quantitative diagnostic method differentiating between healthy and cancerous tissue.

The data analysis is developed on images recorded on human Normal Fat Tissue vs. Well-differentiated (WD) and De-differentiated Liposarcoma (DDLS). Further refinement will allow to detect tumor boundary, diagnose other type of cancer (e.g. breast cancer) where structural analysis is required for diagnosis, or to monitor quantitatively tumor progression during cancer therapy.

As a demonstration of these methods, statistical analysis was developed to evaluate OCT images of human fat specimens. An accurate result was found to quantify healthy vs. cancerous tissue. The analysis can be applied in real-time for diagnosis, and it is much simpler comparing to other quantifying method. This practical advantage gives a good possibility to use in surgical evaluation.

We describe first time a model-based tissue-characterization method based on structural properties of healthy vs. cancerous tissue. Further statistical validation, sensitivity/specificity analysis and classification methods have to be performed on other measurements to prove the efficacy of the developed method.

ACKNOWLEDGEMENTS

The authors wish to acknowledge the very important contribution made by Shang Wang and Narendran Sudheendran. This work was supported by the Hungarian-American Fulbright Commission, the French Ministry of Research and the University of Houston. This work is the continuation of a poster presentation held on November 16, 2012 at the MEGA Research day of the University of Houston.

REFERENCES

Bajraszewski, T., Wojtkowski, M., Szkulmowski, M., Anna Szkulmowska, Huber, R., Kowalczyk, A., 2008. Improved spectral optical coherence tomography using optical frequency comb, *Optics Express*, 16(6).

Brezinski, M. E., 2006. *Optical Coherence Tomography, Principles and Applications*, Academic Press Elsevier Inc.

Drexler, W. and Fujimoto, J. G., 2008. *Optical Coherence Tomography: Technology and Applications*, Springer, Berlin, New York.

Carbajal, E. F., Baranov, S. A., Manne, V. G. R., Young, E. D., Lazar, A. J., Lev, D. C., Pollock, R. E., Larin, K.V., 2011. Revealing retroperitoneal liposarcoma morphology using optical coherence tomography, *Journal of Biomedical Optics*, 16(2).

Fletcher, C. D. M., Rydholm, A., Singer, S., Sundaram, M., Coindre, J. M., 2006. Soft tissue tumours: Epidemiology, clinical features, histopathological typing and grading, *WHO Classification of Soft Tissue Tumors*.

Goldberg, B. D., Iftimia, N. V., Bressner, J. E., Pitman, M. B., Halpern, E., Bouma, B. E., Tearney, G. J., 2008. Automated algorithm for differentiation of human breast tissue using low coherence interferometry for fine needle aspiration biopsy guidance, *Journal of Biomedical Optics*, 13(1),

Gossage, K. W., Tkaczyk, T. T., Rodriguez, J. J., Barton, J. K., 2003. Texture analysis of Optical Coherence Tomography images: feasibility for tissue classification, *Journal of Biomedical Optics*, 8(3).

Gossage, K. W., Smith, C. M., Kanter, E. M., Hariri, L. P., Stone, A. L., Rodriguez, J. J., Williams, S. K., Barton, J. K., 2006. Texture analysis of speckle in Optical Coherence Tomography images of tissue phantoms, *Physics in Medicine and Biology*. 51.

Lahat, G., Madewell, J.E., Anaya, D. A., Qiao, W., Tuvin, D., Benjamin, R. S., Lev, D. C., and Pollock, R. E., 2009. Computed Tomography Scan-Driven Selection of Treatment for Retroperitoneal Liposarcoma Histologic Subtypes, *Cancer* 115(5).

Lev, D., Baranov, S. A., Carbajal, E. F. Young, E. D., Pollock, R. E., Larin, K. V., 2011. Differentiating retroperitoneal liposarcoma tumors with optical coherence tomography, *Proceedings SPIE 7890, Advanced Biomedical and Clinical Diagnostic* Systems IX, 78900U.

McLaughlin, R. A., Scolaro, L., 2010. Parametric imaging of cancer with optical coherence tomography, *Journal of Biomedical Optics*, 15(4).

Miettinen, M. M., 2003. *Diagnostic Soft Tissue Pathology*, Churchill Livingstone.

Miettinen, M. M., 2010. *Modern soft tissue pathology; tumors and non-neoplastic conditions*, Cambridge University Press.

Morris, P., Perkins, A., 2012. Diagnostic imaging, Physics and Medicine 2, *Lancet*, 379.

Mujat, M., R., Ferguson, D., Hammer, D. X., Gittins, C., Iftimia, N., 2009. Automated algorithm for breast tissue differentiation in optical coherence tomography, *Journal of Biomedical Optics*, 14(3).

Rembielak, A., Green, M., Saleem, A., 2011. Pat Price, Diagnostic and therapeutic imaging in oncology, Cancer Biology and Imaging, *Medicine*, 39(12).

Sjöström, P. J., Frydel, Wahlberg, L. U., 1999. Artificial Neural Network-Aided Image Analysis System for Cell Counting, *Cytometry*, 36.

Sullivan, A. C., Hunt, J. P., Oldenburg, A. L., 2011. Fractal analysis for classification of breast carcinoma in Optical Coherence Tomography, *Journal of Biomedical Optics*, 16(6).

Yang, Y., Wang, T., Biswal, N.C., Wang, X., Sanders, M., Brewer, M., Zhu, Q., 2011. Optical scattering coefficient estimated by optical coherence tomography correlates with collagen content in ovarian tissue, *Journal of Biomedical Optics*, 16(9).

Zysk, A. M., Boppart, S. A., 2006. Computational methods for analysis of human breast tumor tissue in optical coherence tomography images, *Journal of Biomedical Optics*, 11(5).